European Journal of Mechanics B/Fluids 45 (2014) 1–11

Contents lists available at ScienceDirect

European Journal of Mechanics B/Fluids

journal homepage: www.elsevier.com/locate/ejmflu

Effect of the vortex dynamics on the drag coefficient of a square back Ahmed body: Application to the flow control

Charles-Henri Bruneau [a,*], Emmanuel Creusé [b], Patrick Gilliéron [c], Iraj Mortazavi [a]

[a] IMB, Université Bordeaux 1, INRIA Bordeaux-Sud-Ouest Equipe MC2, CNRS UMR 5251 351, Cours de la Libération, F-33405 Talence, France

[b] Laboratoire Paul Painlevé, Université Lille 1, INRIA Lille Nord Europe Equipe SIMPAF, CNRS UMR 8524, Cité Scientifique, F-59655 Villeneuve d'Ascq, France

[c] RDMFA, Recherche et Développement en Mécanique des Fluides & Aérodynamique 5, Impasse des Soupirs, F-78640 Neauphle-le-Château, France

ARTICLE INFO

Article history:
Received 21 March 2013
Received in revised form
15 November 2013
Accepted 15 November 2013
Available online 7 December 2013

Keywords:
Vortex dynamics
Pressure forces
Drag control
Ahmed body

ABSTRACT

A vortex generated behind a simplified vehicle induces a pressure force at the back wall that contributes to a significant part of the drag coefficient. This pressure force depends on two parameters: the distance of the vortex to the wall and its amplitude or its circulation. Therefore there are two ways to reduce the drag coefficient: pushing the vortices away from the wall and changing their amplitude or their dynamics. Both analytical studies and numerical simulations show that these two actions decrease the pressure force and consequently reduce the drag coefficient. The first action is achieved by an active control procedure using pulsed jets and the second action is achieved by a passive control procedure using porous layers that change the vortex shedding. The best drag coefficient reduction is obtained by coupling the two procedures.

1. Introduction

A simplified ground vehicle can be represented, as it is often the case both for experiments and numerical simulations by the Ahmed body [1]. It is a three-dimensional bluff body moving in the vicinity of the ground generating a turbulent flow. Several separations appear along the body from the front to the back. The flow behavior is strongly related to the angle of the rear window α. For instance when $\alpha = 25^\circ$ the flow on the rear window is dominated by two strong longitudinal vortices [2,3]. On the contrary when $\alpha = 90^\circ$ the geometry corresponds to a square back Ahmed body, the flow separates at the back and the base flow is no more dominated by longitudinal structures. Experimental and numerical studies confirm this behavior of the detached near-wall flow at the base of the square back Ahmed body geometry [4–7]. Indeed, the vortex shedding generates four mean recirculation zones behind the back wall that are symmetrical with respect to the center of the wall. These recirculation zones contribute to a significant part of the drag coefficient as the vortical structures induce strong pressure forces at the back [8–10]. Thus to get a drag reduction, it is necessary to modify locally the flow, in order to reduce or to push away the strong pressure wells in the near wake [11].

This can be mainly obtained by controlling the flow near the back wall with or without additional energy using active or passive devices [12,13]. On the one hand, an active control consists of adding uniform, pulsed or synthetic jets on the back wall to push away or to split the vortical structures [8,14]. On the other hand a passive control uses fixed devices like rough surfaces, vortex generators or porous layers to change the size and the dynamics of the vortical structures and consequently to reduce the pressure forces [15–19].

However, implementing an efficient control needs to better master the vortex behavior in the very near wake of the obstacle and thus to better understand the relationship between the vortices evolution and the drag forces. An important issue of this relationship is based on the pressure forces generated by the wake vortices on the back wall of the body. It depends on the strength, the size and the trajectory of the vortices in the wake as well as on the speed they are moving away from the back wall.

Some theoretical approaches have been developed considering different simplified kinematic motions in order to better understand the flow behavior [20–22]. From these works, it is possible to calculate the pressure force on the back wall and its evolution with respect to the distance of the vortices from the wall.

However, the viscous vortex dynamics in the wake is much more complex than an ideal vortex convection. Near the wall, the dissipative forces are predominant and the vortices are not directly subject to the inlet velocity. Nevertheless, such a theoretical approach is still helpful showing a general trend related to the

* Corresponding author. Tel.: +33 540006963.
E-mail address: bruneau@math.u-bordeaux1.fr (C.-H. Bruneau).

0997-7546/$ – see front matter © 2013 Elsevier Masson SAS. All rights reserved.
http://dx.doi.org/10.1016/j.euromechflu.2013.11.003

modification of the vortex dynamics. Then the control processes can be directly inspired by the results of the theoretical study as they show the ideal kinematics to get.

In this work, direct numerical simulations of the two-dimensional flow around the square back Ahmed body, corresponding to simplified mono space cars or trucks, are considered. The incompressible Navier–Stokes system is solved in a computational domain including the square back Ahmed body on top of a road at medium Reynolds number. Although the Reynolds number is much lower than the real Reynolds number around ground vehicles, it is possible to study the vortex dynamics and to quantify the effects of the control. First of all, some theoretical results on ideal convective vortex motions are analyzed to compute the resulting pressure force on the wall that depends on two parameters: the distance and the circulation of the vortex. Then, the evolution of a toy vortex added in a background stationary flow is carefully studied without or with an active control by a steady jet. This first study permits to better understand the effect of the control procedure on the kinematics of one vortex and to show the resulting pressure force behaves like the theoretical force computed above.

Finally the vortex shedding of the real flow computed around the body is analyzed as we study the mean trajectory of the top and bottom vortices at the back. Two actions are then implemented to control the flow. The first one involves a closed-loop active control using blowing jets to remove the vortices as fast as possible from the wall. It appears that the control can improve significantly the trajectories and the removal speeds of some vortices to reach almost the ideal motion. The second one involves a passive control using porous layers [19,8,7] in order to change the vortex dynamics in the immediate vicinity of the back wall. The big shedded vortices are replaced by smaller ones with their own dynamics. Consequently the pressure force on the back wall is reduced and finally the drag coefficient is decreased.

This paper is organized as follows. Section two is a recall of the analytical approach showing the link between the removal of vortices from the back wall and the corresponding pressure forces for three different functions. Section three presents briefly the modeling and the numerical simulation. Section four illustrates what is given by the theory with the numerical simulation of a toy vortex added to a steady background flow. In section five a careful analysis of the results obtained by the direct numerical simulation without or with active control is provided. Section six is devoted to the dynamics of smaller shedded vortices and to the passive control procedure that yields a significant drag reduction. Section seven shows that better results can be achieved by coupling active and passive control procedures. At the end some conclusions are deduced.

2. Analytical approach

With non-viscous hypothesis, the two-dimensional vortex model is based on two theories: the circular vortex theory [21,22] and the mirror image vortex theory [20]. The first one considers the vortex as a disk. The velocity is infinite in the center and decreases when the radius increases. To avoid the infinite velocities on the wall, the vortex position is considered to be at least as far as a classical viscous radius value ϵ from the body. The second theory allows to model the vortex sliding actions to the wall. In fact, the sliding force at the wall is the amount of the forces generated by the studied vortex and its wall mirror image vortex. Let us recall here the basis of such an approach and its extension to the force evaluation on the wall.

Let H be the height of the back wall of the obstacle characterized by the coordinates set $x = 0$ and $-H/2 \leq z \leq H/2$ (see Fig. 1). Let us consider $M(0, z)$ a point on the back wall and a vortex whose center is located at point $P(x_1, z_1)$, $x_1 > 0$. The distance between

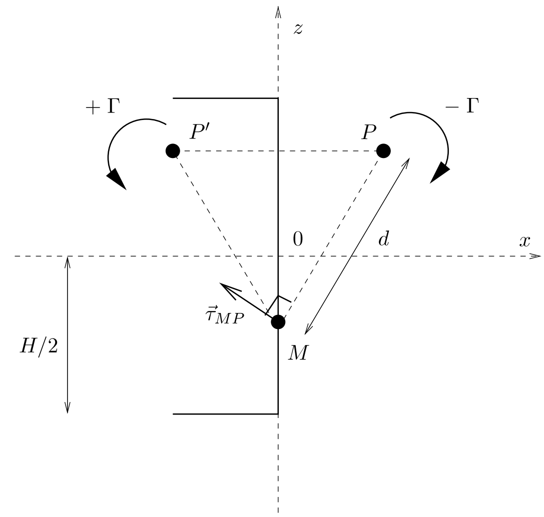

Fig. 1. Location of the vortex center P respecting to the wall.

M and P is denoted d, and $\vec{\tau}_{MP}$ is the unit vector orthogonal to $\overrightarrow{MP}$ given by $\vec{\tau}_{MP} = \overrightarrow{MP}^{\perp} / \|\overrightarrow{MP}\|$. In that case, according to [21], the wall velocity induced at point M by the vortex is given by

$$\vec{V}(M) = \frac{\Gamma}{2\pi d}\, \vec{\tau}_{MP}, \tag{1}$$

where $-\Gamma \in \mathbb{R}$ corresponds to the (negative) vortex circulation. Near the wall, the longitudinal component of the velocity is negligible so the velocity is parallel to the wall. To nullify the normal component of the velocity near the wall, a mirror image vortex has to be located at point $P'(-x_1, z_1)$ with the circulation $+\Gamma$ [20]. The velocity $\vec{W}(M)$ at point M due to this mirror image vortex can be defined in the same way, and a simple calculation shows that the modulus of the resulting velocity $\vec{V}_R(M) = \vec{V}(M) + \vec{W}(M)$ is given by

$$V_R(M) = \|\vec{V}_R(M)\| = \frac{\Gamma\, x_1}{\pi (x_1^2 + (z - z_1)^2)}. \tag{2}$$

According to Bernoulli, the local pressure p with respect to the pressure at rest p_0 is given by

$$p(M) - p_0 = -\frac{\rho}{2} V_R^2(M) = -\frac{\rho}{2} \frac{\Gamma^2\, x_1^2}{\pi^2 (x_1^2 + (z - z_1)^2)^2}, \tag{3}$$

where ρ is the density of the fluid. Consequently, integrating on the back wall, we get the horizontal pressure force F_p induced by the vortex on the whole back of the body:

$$\begin{aligned} F_p &= \int_{-\frac{H}{2}}^{+\frac{H}{2}} -(p(M) - p_0)\, dz \\ &= \frac{\rho}{2} \frac{\Gamma^2}{\pi^2} \int_{-\frac{H}{2}}^{+\frac{H}{2}} \frac{x_1^2}{(x_1^2 + (z - z_1)^2)^2} dz. \end{aligned} \tag{4}$$

Now, if we consider that the vortex is moving, the instantaneous pressure force $F_p(t)$ induced by the vortex on the wall at time t can of course be evaluated by:

$$F_p(t) = \frac{\rho}{2} \frac{\Gamma^2}{\pi^2} \int_{-\frac{H}{2}}^{+\frac{H}{2}} \frac{x_1^2(t)}{(x_1^2(t) + (z - z_1(t))^2)^2} dz. \tag{5}$$

This pressure force depends of course strongly on the circulation Γ but also on the functions $x_1(t)$ and $z_1(t)$. Taking $x_1(t) = \epsilon + t^r$ with $1/2 \leq r \leq 2$ and $\epsilon = \sqrt{\Gamma^2 \rho / p_0}$ (see [21]), and considering in a first approach an horizontal evolution ($z_1(t) \equiv 0$), some

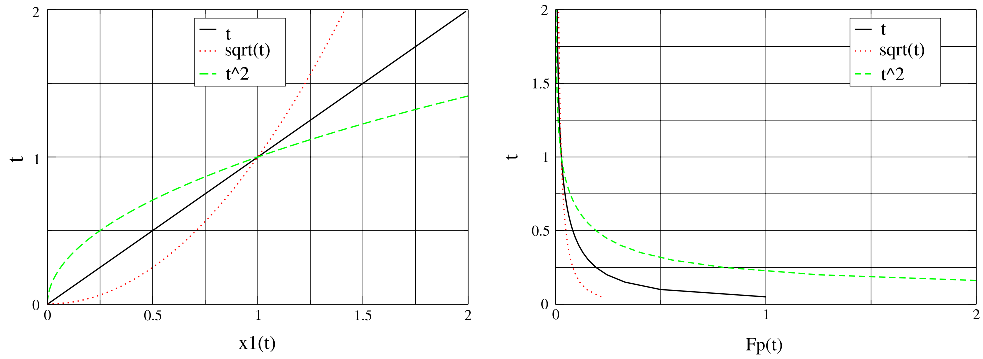

Fig. 2. Vortex trajectory evolutions (left) and corresponding pressure forces (right).

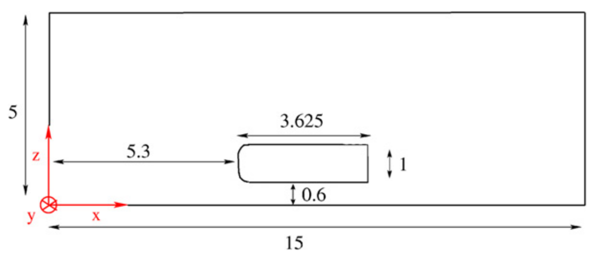

Fig. 3. Computational domain around the square back Ahmed body.

characteristic behaviors of the vortex trajectories behind the back wall can be represented according to r. In Fig. 2, $x_1(t)$ and $F_p(t)$ are represented for $r = 1/2, r = 1$ and $r = 2$. As expected, the best result (yielding the lowest force) is achieved for $r = 1/2$ as it corresponds to the fastest removal from the wall at $t = 0$. At the beginning of the evolution the difference of the forces is tremendous and so the way the removal occurs has a huge effect on the pressure force at the back and consequently on the drag coefficient.

In the following, we shall first consider the actual trajectory of one vortex superimposed on a given background flow, and its moving away from the back of the body. The goal is to investigate the r parameter characterizing this vortex removal from the body, both for an uncontrolled and an active controlled simulation. Then, the effect of some control devices on the vortices trajectories in the case of a real flow will be studied. The interest of this point is to understand on which area of the flow the control processes involved are able to effectively drive the vortices trajectories, and so to decrease the drag coefficient.

3. Modeling and numerical simulation

3.1. Uncontrolled flow

The aim is to simulate and control the flow around the square back Ahmed body ($H = 1$). The simulation is performed in the computational domain $\Omega = (0, 15H) \times (0, 5H)$ with the body located at the distance $5.3H$ from the entrance section and $0.6H$ from the road (Fig. 3) and whose length is $L = 3.625H$, by solving the penalized Navier–Stokes equations in velocity and pressure (U, p) (see [23,18]). By using H and $\|\overline{U}\|$ (the norm of the mean velocity) in the adimensioning process, these ones are given in their dimensionless form by:

$$\partial_t U + (U \cdot \nabla)U - \frac{1}{\mathrm{Re}}\Delta U + \frac{U}{K} + \nabla p = 0 \quad \text{in } \Omega_T = \Omega \times (0, T), \tag{6}$$

$$\operatorname{div} U = 0 \quad \text{in } \Omega_T, \tag{7}$$

where $K = \frac{k\Phi\overline{U}}{\nu H}$ is the non dimensional coefficient of permeability of the medium, k is the intrinsic permeability, ν is the kinematic viscosity, Φ is the porosity of the fluid and $\mathrm{Re} = \frac{\|\overline{U}\|H}{\nu}$ is the Reynolds number based on the height of the body and the mean velocity. From now, all variables have consequently to be understood as dimensionless ones. To recover the genuine Navier–Stokes equations we set $K = 10^{16}$ in the fluid. On the contrary $K = 10^{-8}$ in the solid body to get a velocity field of the same order in the solid mimicking a porous body with very low permeability. These values are set on the staggered velocity points of a Cartesian mesh according to their location. The equations are coupled to an initial datum corresponding to the flow at rest and to two kinds of boundary conditions. A constant Dirichlet condition is imposed upstream and on the road $\overline{U} = (\overline{u}_x, \overline{u}_z) = (1, 0)$ (corresponding to the speed of the ground vehicle) and a non reflecting boundary condition on the open frontiers (top and downstream) [24] is used.

The system of Eqs. (6), (7) is solved by a strongly coupled approach for the physical unknowns (U, p). The time discretization is achieved using a second-order Gear scheme with explicit treatment of the convection term. All the linear terms are treated implicitly and discretized via a second-order centered finite differences scheme. The CFL condition related to the convection term requires a time step of the order of magnitude of the space step as $\overline{U} = (1, 0)$, which is relevant to have a good accuracy of the evolution of the flow and does not induce too much cpu time. A third-order finite differences upwind scheme is used for the discretization of the convection terms [25]. The efficiency of the resolution is obtained by a multigrid procedure using V cycles and a cell-by-cell relaxation smoother. A set of grids is defined starting from the 15×5 coarse mesh to the finest mesh and the number of grids is determined to get accurate results.

To choose a relevant number of grids in order to get reliable results we first perform numerical tests on four consecutive finest grids, namely a 480×160, a 960×320, a 1920×640 and a 3840×1280 cells uniform mesh. The flow around the square back Ahmed body is computed on these four consecutive meshes at $\mathrm{Re} = 8276$ corresponding to Reynolds number 30 000 based on the body length. The drag coefficient C_D is presented in Table 1. We see clearly that the results are very different from one grid to another except for the two finest grids that give much closer results. So until the end of this paper the results will be presented in two dimensions on the 1920×640 cells uniform mesh that insures that grid convergence is reached.

3.2. Active and passive controlled flows

To remove the vortices from the back wall, an active control with blowing jets is used. The first choice is to take a constant jet of velocity $U_j = 0.6\overline{U}$ which corresponds to the forcing intensity 8×10^{-3} defined by $C_\mu = \frac{h_j}{H}\left(\frac{U_j}{\overline{U}}\right)^2$ where h_j is the size of the jet [8].

Table 1
Values of the drag coefficient C_D on four consecutive grids.

Cartesian mesh	C_D
480 × 160	0.46
960 × 320	0.95
1920 × 640	1.52
3480 × 1280	1.56

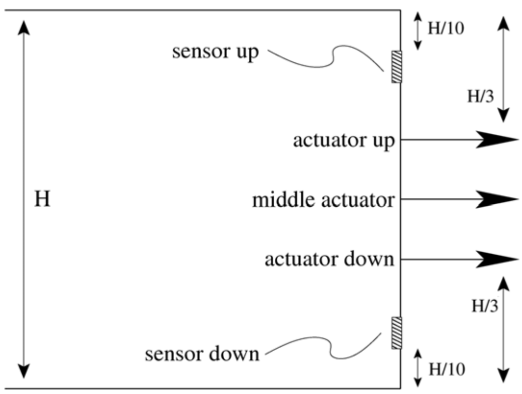

Fig. 4. Position of the actuators and sensors at the back wall of the square back Ahmed body.

Fig. 5. Position of the porous layer on the roof of the square back Ahmed body.

But, as the effect of the vortices is strongly linked to the pressure at the wall, an efficient choice for such a control is a closed-loop active control with the velocity of the blowing jets U_j given by:

$$U_j = \frac{U_{j\max}}{2}(1 - \beta(p_{\text{sensors}} - \bar{p}_{\text{sensors}})), \tag{8}$$

where $U_{j\max}$ is the maximum blowing velocity (here $U_{j\max} = 1.2\overline{U}$ to get the same mean velocity as for the constant jet), β a normalized coefficient defined in such a way that $0 \le U_j \le U_{j\max}$ (here $\beta = 1.5$), $p_{\text{sensors}} = \min(p_{\text{sensor1}}, p_{\text{sensor2}})$ the lowest pressure measured by the sensors and $\bar{p}_{\text{sensors}}$ the averaged pressure of both sensors [8], where the sensors' location is shown in the Fig. 4. The closed-loop active control techniques used in this work are composed of a jet in one of the three positions of the back wall (see Fig. 4).

On the other hand, to modify the vortex shedding and especially to change the size and the dynamics of the vortices a passive control using porous slices is implemented. With the penalized Navier–Stokes equations it is very easy to handle as it is only necessary to change the value of K by setting $K = 10^{-1}$ in the porous region (see [18] for more details). Here we use only a porous layer on the upper part of the body as shown in the Fig. 5.

4. Kinematics and active control of a toy vortex

The real wake behind a bluff body like Ahmed body is composed of vortical structures with different circulations and periods of shedding depending mainly on the Reynolds number as the geometry is given. They have a reciprocating interaction with the near wake flow feeding the vortex street generation and being themselves conditioned by the former generated vortices. However, even if these vortices interactions are very complex, their main characteristics can be mimicked by simplified kinematic verifications based on the vortex trajectories and their speed of removal from the wall [26]. Previous studies have shown that the flow behind a bluff body can be divided into two main areas: the vortex formation area and the transport area [27]. Here we focus on the transport of vortices in the near wake as their shedding is mainly due to the geometry and the Reynolds number.

In this section, in order to better understand the effect of the shedding vortices on the body forces, a toy vortex is superimposed to a steady background flow obtained at low Reynolds number Re = 200. The velocity of this toy vortex is defined by

$$\begin{cases} u_x(x,z) = -\dfrac{\gamma_1}{2R_1}(z - z_1)e^{-a\left(\frac{r_1}{R_1}\right)^n}, \\ u_z(x,z) = \dfrac{\gamma_1}{2R_1}(x - x_1)e^{-a\left(\frac{r_1}{R_1}\right)^n}, \end{cases} \tag{9}$$

where γ_1 is the amplitude of the vortex, R_1 its radius, (x_1, z_1) the location of its center, $r_1^2 = (x - x_1)^2 + (z - z_1)^2$, and where a and n are real parameters to be specified. In this section we take $\gamma_1 = 1.5$, $R_1 = 0.15$, $(x_1, z_1) = (9.3, 0.85)$, $a = 0.2$ and $n = 6$. Let us recall that the back wall is located at $x = 8.925$ with z between 0.6 and 1.6 in the numerical simulation. In the Fig. 6, the evolution of this toy vortex at the very beginning at $t = 0.2$ and later at $t = 5$ is shown at Reynolds number Re = 1000. Due to its proximity to the back wall of the Ahmed body, the vortex interacts with the wall to yield a dipole which moves away at the bottom and does not induce a significant pressure force, and a strong vortex moving upwards. The motion of this new vortex is followed from

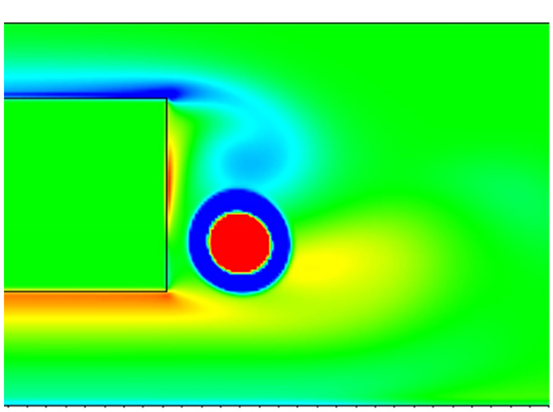

(a) $t = 0.2$.

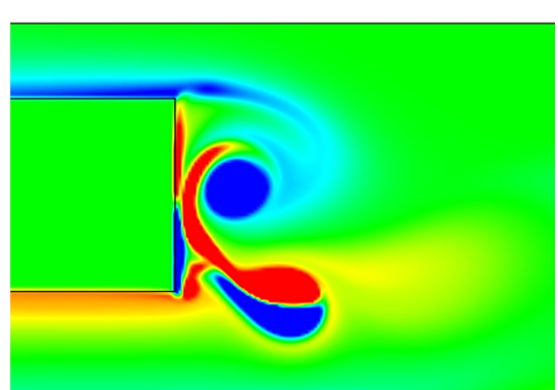

(b) $t = 5$.

Fig. 6. New vortex evolution before starting the comparison.

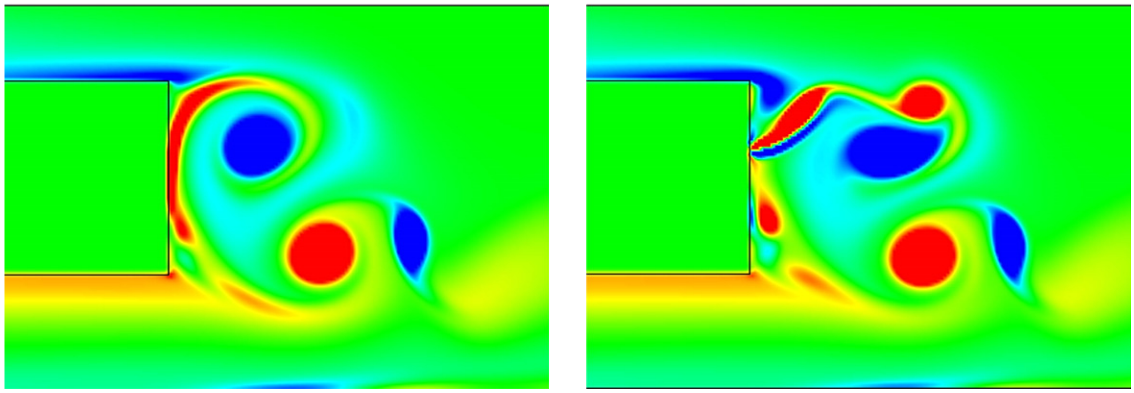

(a) Uncontrolled case. (b) Controlled case.

Fig. 7. Comparison of the vorticity field in the wake of Ahmed body between the uncontrolled and the controlled cases at simulation time $t = 12$.

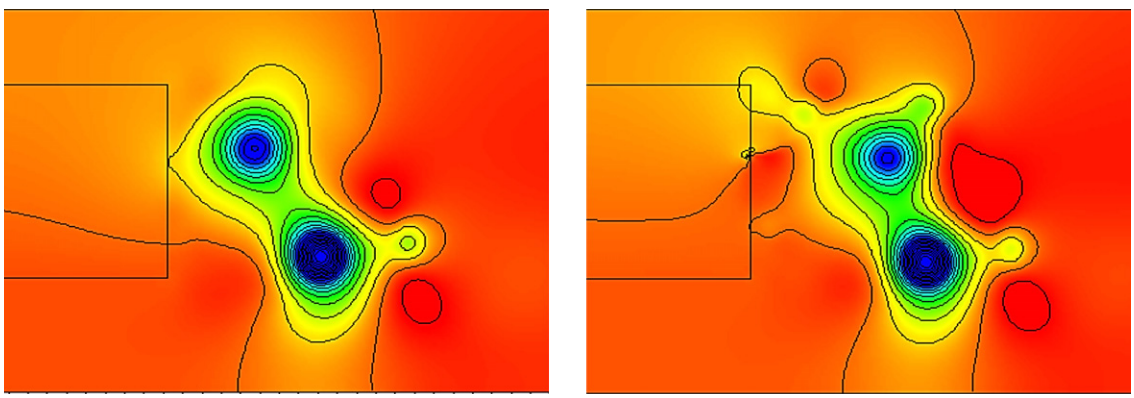

(a) Uncontrolled case. (b) Controlled case.

Fig. 8. Comparison of the pressure field in the wake of Ahmed body between the uncontrolled and the controlled cases at simulation time $t = 12$.

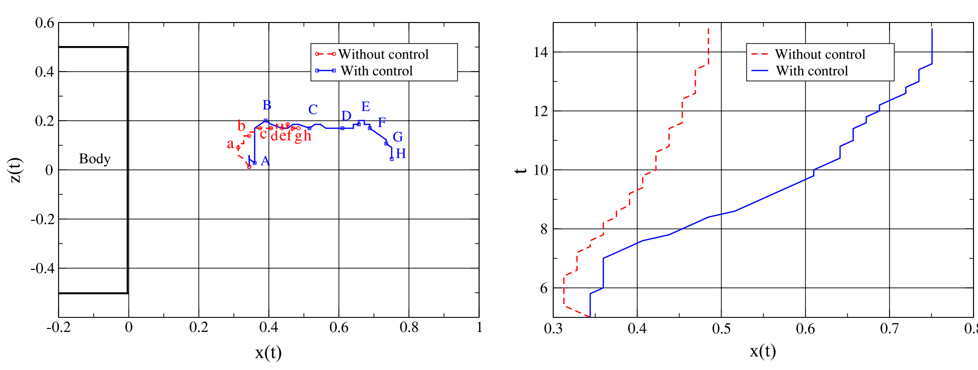

Fig. 9. Comparison of trajectories and removals from the wall of the new vortex.

simulation time $t = 5$ to simulation time $t = 15$, its trajectory as well as the resulting pressure force at the back are computed for both the uncontrolled and the controlled cases, here the control is performed by blowing with a steady jet $(u_x, u_z) = (0.6, 0)$ at the up actuator. In the Figs. 7 and 8 are plotted the vorticity and pressure fields in the wake of the Ahmed body at simulation time $t = 12$. The dipole moves away at the bottom of the body and has almost no influence on the body. In addition there is a very small difference in this dipole behavior between the uncontrolled and the controlled cases. So the difference of the pressure force and of the drag are mainly due to the new vortex and the blowing jet. This new vortex has still a very strong impact on the body as it can be seen in both figures for the uncontrolled case (the deep pressure well is still interacting with the body). On the other hand, in the controlled case, the jet has pushed away the new vortex and thus its influence has decreased a lot. But the jet itself induces a pressure force on the back that is not negligible. Therefore to have a decrease of the drag coefficient a strong variation of the pressure force induced by the new vortex is necessary. Let us see now the difference of trajectories and removals from the wall for both cases. They are illustrated in the Fig. 9, the letters corresponding to the position of the center of the vortex at various simulation times

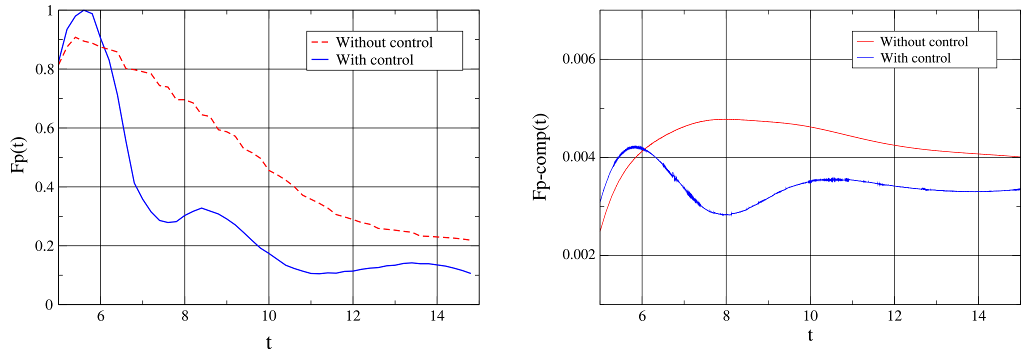

Fig. 10. History of the theoretical pressure force $F_p(t)$ and of the pressure force computed from the numerical simulation at the back $F_{p-\mathrm{comp}}(t)$ induced by the new vortex between simulation times $t = 5$ and $t = 15$.

Table 2
Time-letters correspondences for the toy vortex in the real flow.

Points without control	*a*	*b*	*c*	*d*	*e*	*f*	*g*	*h*
Points with control	*A*	*B*	*C*	*D*	*E*	*F*	*G*	*H*
Simulation time *t*	6	7	8	9	10	11	12	13

given in Table 2. At its creation the new vortex moves upwards as it is created with an upward speed and it is also pushed by the flow between the body and the road. At simulation time $t = 5$ the vortex starts from the same position and moves on upwards until time $t = 7$. Then the flow alone (uncontrolled case) or the flow plus the blowing jet (controlled case) push it away from the back wall. We can see clearly on these plots the huge difference between the two cases. The removal has almost a square root behavior from time $t = 7$ to time $t = 10$ for the controlled case whereas it is linear for the uncontrolled case. So, at time $t = 10$, the vortex has moved away from its initial position of $d = 0.28$ of the height of the body instead of $d = 0.08$ without control. This makes at the end a big difference in the normalized pressure force $F_p(t)$ and on the pressure force computed from the numerical simulation at the back (see Fig. 10). Here, the force $F_p(t)$ is computed similarly to (5) by neglecting the boundary layer thickness as the velocities and the height the of Ahmed body are small enough. It is now given by

$$F_p(t) = \frac{\rho\,\gamma_1^2}{2\,R_1^2}\int_{-H/2}^{H/2} x_1^2(t)\; e^{-2a((x_1^2(t)+(z-z_1(t))^2)/R_1^2)^{n/2}}\,dz. \qquad (10)$$

Both forces have a similar behavior along time and show the same difference magnitude between the uncontrolled and controlled cases. As the pressure force at the back induces about 60% of the drag coefficient, the resulting C_D with control is nearly 20% smaller. This reduction is obtained despite the fact that the jet induces a drag coefficient of about 0.004 which represents for this simple flow one third of the total drag coefficient. This shows that this technique can be used to push away the vortices and may be to reduce the drag coefficient in a real flow as we shall see in the next section.

5. Kinematics and active control of a real flow

In this section, the effect of control on the vortex kinematics is studied first with an instantaneous approach, and then for averaged flow fields. All the computations are performed at Reynolds number Re = 8276 from now to the end of the paper.

Instantaneous vortex motion

A first analysis consists in comparing the instantaneous vorticity fields of the reference (uncontrolled) case to the controlled case

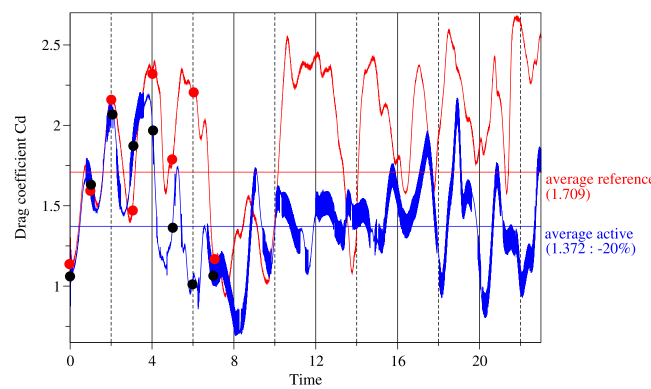

Fig. 11. Evolution and mean value of the drag coefficients for the reference case and the controlled case with a closed-loop active control at the middle of the wall.

with one actuator in the middle of the back wall. This position is chosen in order to take into account the shedding that generates both up and down vortices. Two simulations are initialized with the same reference flow in order to observe the evolution of up and down vortical structures. The first case is without control and the second is with control corresponding to a blowing closed-loop actuator which better includes the shedding frequencies of the real flow. The Fig. 11 shows the time evolution and the averaged values of the drag coefficients for both cases. After two periods of shedding, the drag coefficient is considerably reduced (−20%) by the blowing control.

The Figs. 12 and 13 represent the instantaneous vorticity fields for eight successive moments. The control becomes effective after $t = 3.0$ and up to this time the fields are almost identical. Then, the vortices are pushed away more quickly in the controlled case as it can be seen at simulation time $t = 5.0$ for a top vortex and at time $t = 6.0$ for a bottom vortex. To better analyze the efficiency of the control, in the Fig. 14 the trajectories of two top and bottom vortices with the same initial position are compared for the uncontrolled and controlled cases. The letters $A-H$ and $a-h$ correspond to the same times in the trajectories for both simulations (see Table 3). As the figure shows, the blowing jet pushes away very quickly the vortical structures from the back wall whereas in the uncontrolled simulation these vortices move away slowly in the near wake of the wall.

Averaged vortex motion

In order to get a quantitative estimation of the relationship between the vortex kinematics and the drag reduction due to the control, an averaged estimation of several vortex motions is necessary. So the mean trajectories of the top and bottom vortices are studied for uncontrolled and controlled cases. The averaging

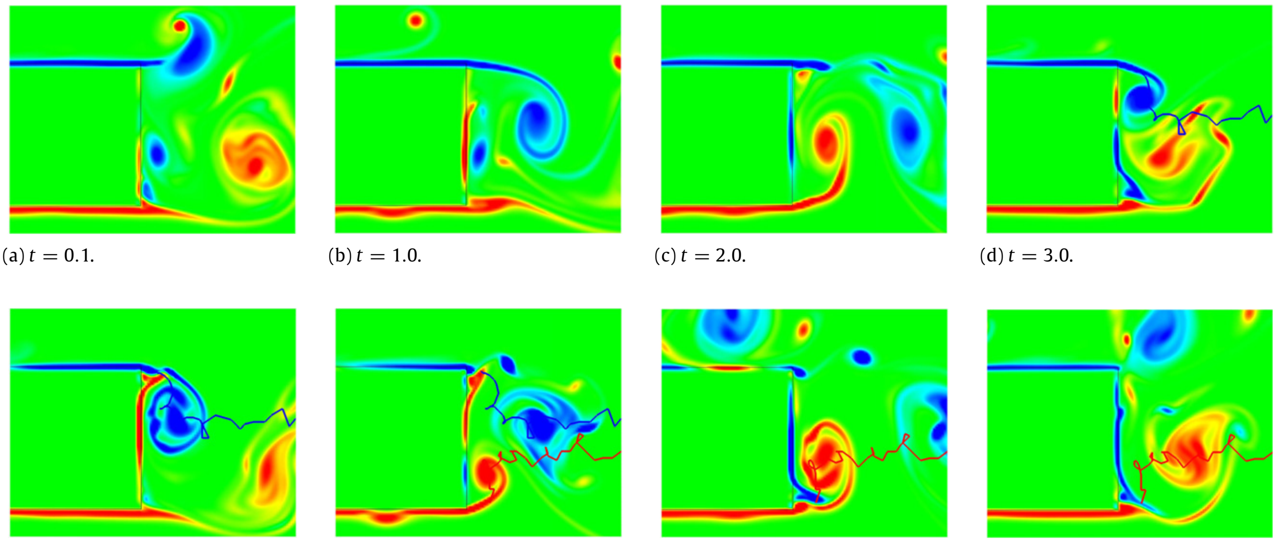

(a) $t = 0.1$. (b) $t = 1.0$. (c) $t = 2.0$. (d) $t = 3.0$.

(e) $t = 4.0$. (f) $t = 5.0$. (g) $t = 6.0$. (h) $t = 7.0$.

Fig. 12. Vorticity fields along time for the reference case without control.

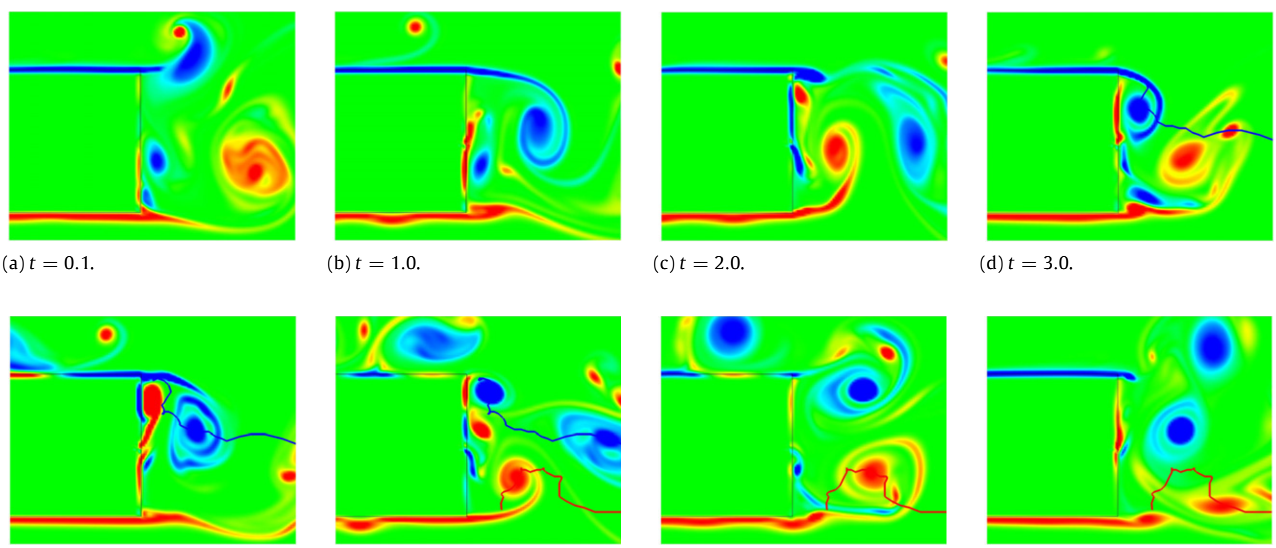

(a) $t = 0.1$. (b) $t = 1.0$. (c) $t = 2.0$. (d) $t = 3.0$.

(e) $t = 4.0$. (f) $t = 5.0$. (g) $t = 6.0$. (h) $t = 7.0$.

Fig. 13. Vorticity fields along time for the controlled case with a closed-loop active control at the middle of the wall.

Table 3
Time-letters correspondences for the instantaneous vortex motion study.

Points	*A*	*B*	*C*	*D*	*E*	*F*	*G*	*H*	*a*	*b*	*c*	*d*	*e*	*f*	*g*	*h*
Simulation time t	2.5	3.0	3.5	4.0	4.5	5.0	5.5	6.0	5.0	5.5	6.0	6.5	7.0	7.5	8.0	8.5

procedure is performed for ten successive vortices on both sides of the wall from simulation time $t = 3$ until time $t = 23$. In the Fig. 15 the mean uncontrolled trajectories are compared to the mean controlled ones with a closed-loop actuator at the middle of the back wall. The time-letters correspondences are given in Table 4, time $t = 0$ corresponds to the first time a vortex is identified by Weiss criterion [28] in the vicinity of one corner. This statistical study reveals that the control has no effect on the top vortices removal as they are naturally driven away by the flow. However, the trajectories of the bottom vortices are drastically modified as in the reference flow, the bottom vortices are pushed upwards by the flow underneath the body. In that case, like for the toy vortex study, the vortices are expelled from the body very quickly with the control. The Fig. 16 shows the top vortices have almost the same removal for the uncontrolled and controlled cases. On the other hand, the bottom vortices have a tremendous change. For the uncontrolled case they are removed from the wall with a square law whereas for the controlled case the removal follows a linear law. These statistical results confirm the efficiency of the active control on the removal of vortices. We shall see in the last section to what amount this can yield a drag coefficient reduction.

6. Change of vortex shedding by passive control and resulting vortex dynamics

As seen in Section 2 the pressure force at the back depends strongly on the circulation Γ of the vortices. An idea to change the

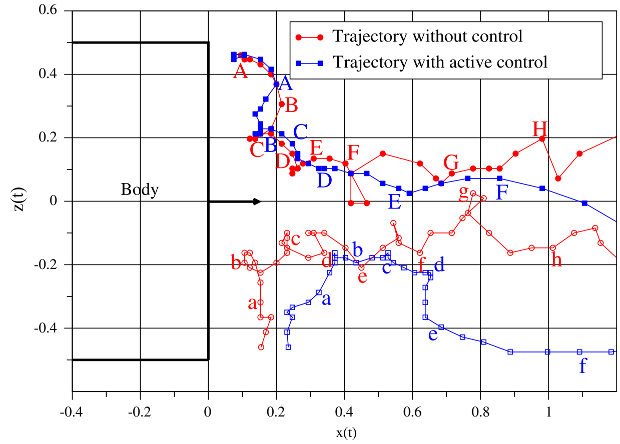

Fig. 14. Comparison of trajectories for the top and bottom vortices without control and with a closed-loop active control at the middle of the wall.

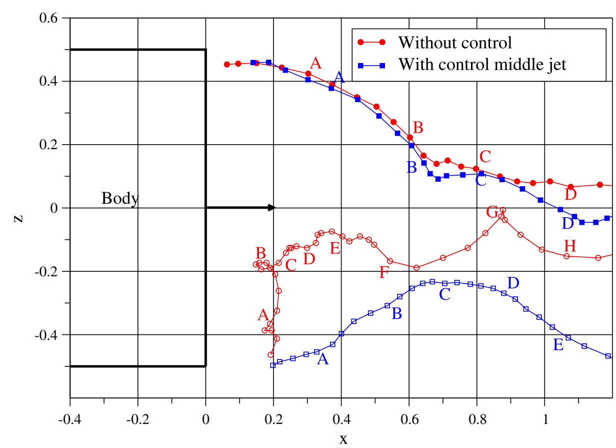

Fig. 15. Comparison of averaged trajectories for the cases without control and with a closed-loop active control at the middle of the wall.

Table 4
Time-letters correspondences for the averaged vortex motion study.

Points	*A*	*B*	*C*	*D*	*E*	*F*	*G*	*H*
Time *t*	0.5	1.0	1.5	2.0	2.5	3.0	3.5	4.0

circulation is to change the shedding of vortices by breaking the vortices into smaller ones. A way to do that is to use porous layers on top of the body for instance (see [19]) as shown in the Fig. 5. Indeed, due to the slow laminar flow inside the porous layer, there is a Kelvin–Helmholtz instability that generates small eddies on the roof and consequently the size of the shedded vortices in the near wake is drastically reduced.

Ideal dynamics of small vortices

Here, we propose to analyze the influence of changing the size and the dynamics of the shedded coherent structures. To make this analysis we still use the toy vortex introduced in Section 4 in its genuine form (9). A simple calculation shows that the circulation generated by this vortex along the circle of radius R_1 is given by:

$$\Gamma_{R_1} = \int_{r=R_1} \vec{u}\cdot\vec{\tau}\, dl = \pi\gamma_1 R_1 e^{-a}. \qquad (11)$$

Moreover, using Bernoulli's law (see Section 2), and assuming that $x_1 = R_1$ and $z_1 = H/4$, the pressure force induced by the vortex on the back of the Ahmed body is similar to (10):

$$F_p^{(1)} = \frac{\rho\,\gamma_1^2}{2}\int_{-H/2}^{H/2} e^{-2a(r/R_1)^n}\, dz,$$

where $r^2 = R_1^2 + (z - H/4)^2$. This pressure force decreases rapidly when the vortex moves away from the wall and is almost zero as soon as the vortex is one diameter downstream to the wall.

We assume now that this large vortex is split into smaller vortices that are distributed around its circumference (see Fig. 17 for $N = 2$ and $N = 4$) as it was observed in [19] and can be seen below in the Fig. 19 at time $t = 5.5$ for instance. These small vortices fill the same place as the unique vortex and follow globally the same trajectory. So to compare their effect on the back wall, it is sufficient to compare the mean forces at a given position and a given time. In that case only the closest vortex induces a significant pressure force on the wall. We assume moreover that each of the N created small vortex ($N \geq 2$) has the same radius R_N defined by $R_N = \alpha R_1/N$, where $0 < \alpha < 1$. Consequently, the coordinates of the center of the kth small vortex are given by:

$$\begin{cases} x_k^{(N)}(\theta) = R_1 + R_1\left(1 - \dfrac{\alpha}{N}\right)\cos\left(\theta + \dfrac{2k\pi}{N}\right), \\ z_k^{(N)}(\theta) = \dfrac{H}{4} + R_1\left(1 - \dfrac{\alpha}{N}\right)\sin\left(\theta + \dfrac{2k\pi}{N}\right), \end{cases}$$

where θ corresponds to the rotation of the global structure defined by the N small vortices ($0 \leq \theta \leq 2\pi$), and where $0 \leq k \leq N - 1$.

Assuming that this phenomenon obeys a conservative principle of the circulation, we obtain from (11) that the amplitude γ_N of each of these small vortices is given by:

$$N\,\gamma_N\, R_N = \gamma_1\, R_1,$$

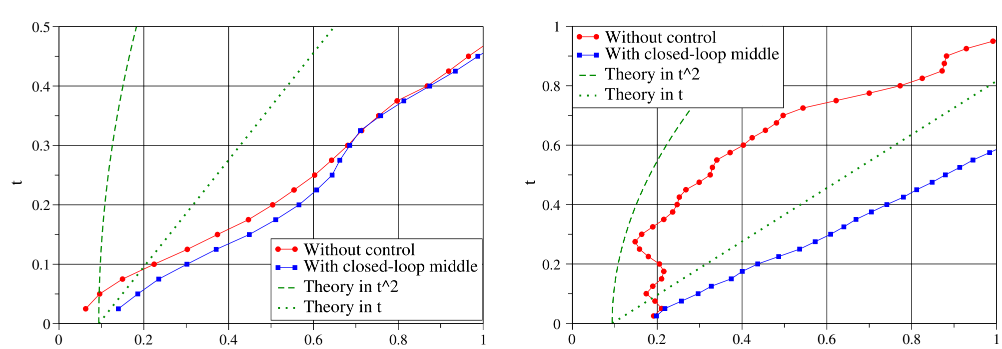

(a) Top vortices. (b) Bottom vortices.

Fig. 16. Comparison of averaged removals from the wall for the cases without control and with a closed-loop active control at the middle of the wall.

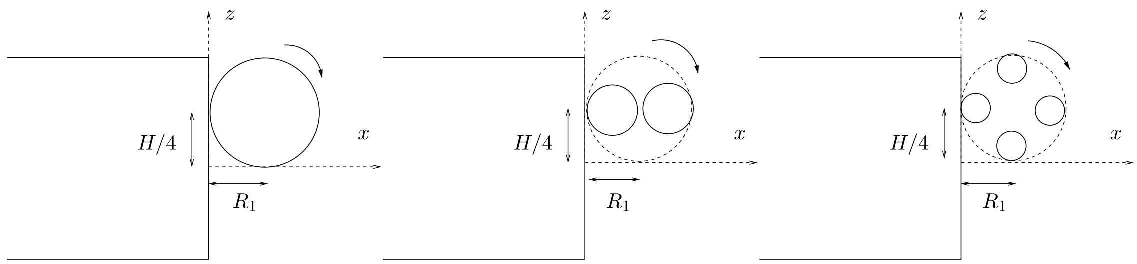

Fig. 17. Location of the initial vortex (left) and the corresponding small vortices for $N = 2$ (middle) and $N = 4$ (right), in the case $\alpha = 1$ and $\theta = 0$.

in other words:

$$\gamma_N = \frac{\gamma_1}{\alpha}.$$

Consequently, each vortex has a smaller radius, but a larger amplitude than the previous one. The dynamics of the smaller vortices constitutes a set of rotating vortices as shown in the Fig. 17. At a given position θ, the pressure force induced by the N small vortices on the back of the Ahmed body is:

$$F_p^{(N)}(\theta) = \frac{\rho\,\gamma_N^2}{2\,R_N^2} \sum_{k=0}^{N-1} \int_{-H/2}^{H/2} (x_k^{(N)}(\theta))^2\, e^{-2a(r_{k,N}(\theta)/R_N)^n}\, dz,$$

where $r_{k,N}^2(\theta) = (x_k^{(N)}(\theta))^2 + (z - z_k^{(N)}(\theta))^2$. It remains to evaluate the average value of $F_p^{(N)}(\theta)$ when the whole structure is turning on itself, which is finally given by:

$$\overline{F}_p^{(N)} = \frac{1}{2\pi} \int_0^{2\pi} F_p^{(N)}(\theta)\, d\theta.$$

We plot in the Fig. 18 the value of $\overline{F}_p^{(N)}/F_p^{(1)}$ versus N, for several values of α ($\alpha = 1.00$, $\alpha = 0.5$, $\alpha = 0.25$ and $\alpha = 0.125$), for $a = 0.2$ and $n = 6$ (another choice would lead to very similar results). We see that whatever the number of vortices $N \geq 2$ and the value of the parameter $0 \leq \alpha \leq 1$ are, the pressure force at the back of the body is considerably reduced, which is clearly an important saving. The more vortices there are (and consequently the smaller they are), the larger the reduction of the pressure force on the body. Of course, the real phenomenon is more complex, as the set of smaller vortices is not globally stationary just behind the body and uniformly rotating on itself. It is subject to diffusion and convection forces. Nevertheless, we claim that this simple analysis allows to give an explanation to the fact that the passive control, by splitting large vortices into smaller ones as explained above, can give rise to a significant drag reduction.

Passive control of a real flow

Here, we compute the flow around the square back Ahmed body when a porous layer has been added on top of the roof as shown in the Fig. 5. For the uncontrolled case in the Fig. 12, there is the shedding of large vortices generated at the corners of the body which remain in the immediate vicinity of the back wall and thus generate a strong pressure force before to be carried away by the convective process. These vortices are responsible for a large part of the drag coefficient. When a porous layer is added on top of the body there are still such vortices at the bottom but, due to the Kelvin–Helmholtz instability between the low laminar flow inside the porous layer and the fluid flow, small vortices develop on top of the porous layer and the big shedded vortex is replaced by several smaller vortices that turn around clockwise. In particular the four vortices at time $t = 5.5$ in the Fig. 19 occupy the same place as the single vortex in the uncontrolled case as assumed in the subsection above. As these vortices are turning around, only one of them is sometimes close enough to induce a significant pressure force, the others are more than a diameter away. So, with this passive control, a 20% drag reduction was numerically observed in [8].

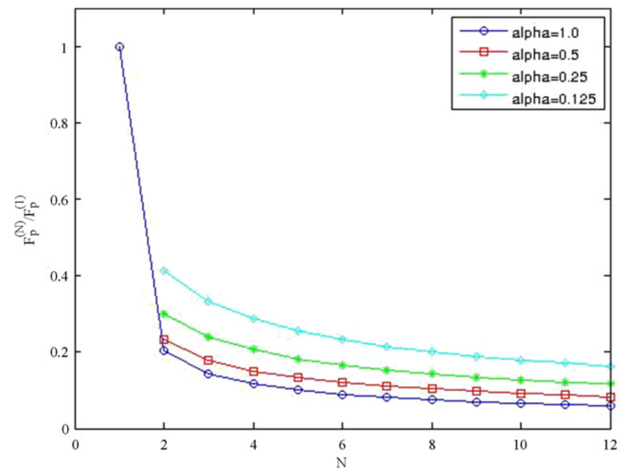

Fig. 18. $\overline{F}_p^{(N)}/F_p^{(1)}$ versus N for $\alpha = 1.00$, $\alpha = 0.5$, $\alpha = 0.25$ and $\alpha = 0.125$.

7. Application of both control procedures to reduce the drag coefficient of the square back Ahmed body

As seen in the previous sections, it is possible to make actions on the flow to decrease the pressure force at the back of the Ahmed body and thus to a significant reduction of the drag coefficient. We have shown in Section 5 that a closed-loop active control is very efficient on the strong bottom vortices as their natural trajectory goes upwards due to the jet flow between the body and the road. However the same control is not so efficient on the top vortices as their natural trajectory follows the main flow and are not trapped by the recirculation zone like the bottom ones. For these top vortices, we have shown in Section 6 that a more appropriate action is to add a porous layer on top of the roof of Ahmed body as shown in the Fig. 5. Indeed, the shedding as well as the vortex dynamics of the top vortices are drastically changed and consequently the pressure force at the back is reduced.

The idea is therefore to couple a closed-loop active control with a down blowing jet at a distance $H/3$ from the bottom edge and a passive control using a porous layer on the roof. The improvement of such a technique can be seen in the Fig. 20 on the trajectories and removals. The mean trajectory of the bottom vortices is further to the back wall than in the previous active control at the middle of the back and thus the removal is now closer to the ideal case in square root. In addition, due to the passive control with a porous layer on the roof, the vortices are smaller and their dynamics induces lower pressure forces at the back. Consequently the mean drag force at the back is reduced up to 46% and thus a 31% drag reduction is achieved.

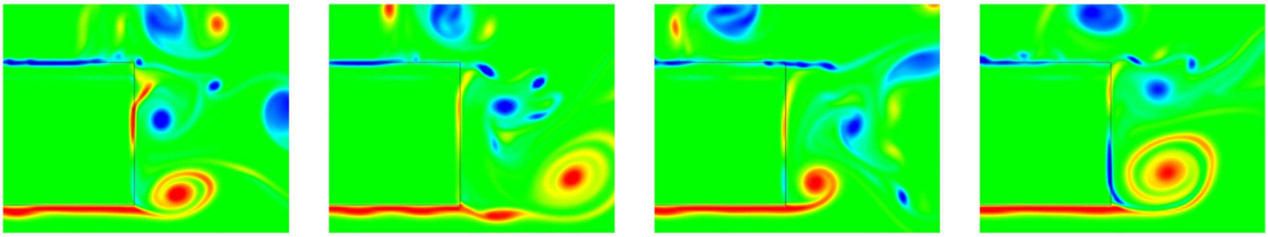

(a) $t = 4.0$. (b) $t = 5.5$. (c) $t = 6.6$. (d) $t = 8.3$.

Fig. 19. Evolution of the vorticity field during one shedding cycle of the controlled flow by one porous layer on top of the body.

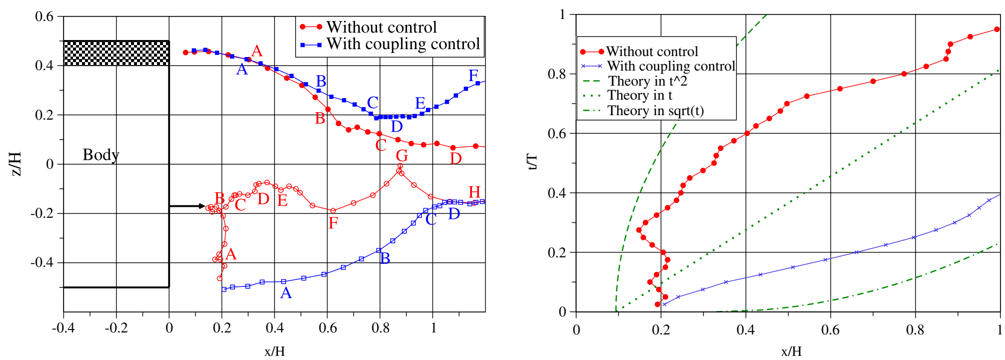

(a) Trajectories. (b) Removals.

Fig. 20. Comparison of averaged trajectories and removals for the uncontrolled flow and the coupling controlled flow.

8. Conclusions

In the first part of this paper, the drag effect of theoretical vortices moving away from a wall with analytical laws is studied. It is shown that the magnitude of the pressure forces on the wall depends directly on the speed of removal of the vortices downstream and their circulation. The larger this speed is, the more the pressure forces decrease and so the drag coefficient. This is confirmed by numerical simulations using a toy vortex.

Then a closed-loop active control is used to reduce the drag coefficient of the square back Ahmed body. It is confirmed that such an active control is efficient for some vortices according to their trajectory. It is the case for the shedded vortices coming from the bottom edge of the back wall due to the presence of the road but there is no noticeable improvement on the top vortices.

A passive control using a porous layer on the roof is able to change the size and the dynamics of the top vortices reducing also significantly the drag forces. Finally, coupling the two control techniques permits to change drastically the pressure forces at the back and to get a 31% reduction of the drag coefficient. Although the simulations were performed at quite low Reynolds number compared to the real flow, the results of the control are close to those obtained in [29] at $Re = 2.8 \times 10^6$.

Acknowledgment

The authors would like to thank Harsh Parekh for the improvement of some figures. The simulations were run on PLAFRIM platform supported by IMB University of Bordeaux and INRIA Bordeaux - Sud Ouest.

References

[1] S.R. Ahmed, G. Ramm, G. Faltin, Some Salient Features of the Time-Averaged Ground Vehicle Wake, SAE-Paper, 840300, 1984.
[2] Ch.-H. Bruneau, P. Gilliéron, I. Mortazavi, Flow manipulation around the Ahmed body with a rear window using passive strategies, Comptes Rendus - Mécanique 335 (4) (2007).
[3] C.-H. Bruneau, E. Creusé, D. Depeyras, I. Mortazavi, P. Gilliéron, Active procedures to control the flow past the Ahmed body with a 25° rear window, Int. J. Aerodynamics 1 (3/4) (2011).
[4] A. Brunn, E. Wassen, D. Sperber, W. Nitsche, F. Thiele, Active drag control for a generic car model, in: King (Ed.), Active Flow Control, Notes on Numerical Fluid Mechanics and Multidisciplinary Design, Vol. 95, 2007, pp. 247–259.
[5] P. Gilliéron, F. Chometon, Modeling of stationary three-dimensional separated air flows around an Ahmed reference model, ESAIM Proc. 7 (1999).
[6] S. Krajnović, L. Davidson, Numerical study of the flow around the bus-shaped body, ASME J. Fluids Eng. 125 (2003).
[7] M. Rouméas, Contribution à l'analyse et au contrôle des sillages de corps épais par aspiration ou soufflage continu, Ph.D. Thesis, 2006.
[8] C.-H. Bruneau, E. Creusé, D. Depeyras, I. Mortazavi, P. Gilliéron, Coupling passive and active techniques to control the flow past the square back Ahmed body, Comput. Fluids 38 (10) (2010).
[9] P. Gilliéron, A. Spohn, Flow separations generated by a simplified geometry of an automotive vehicle, in: IUTAM Symp. Unsteady Separated Flows, 2002.
[10] M. Onorato, A.F. Costelli, A. Garonne, Drag measurement through wake analysis, SAE Paper, vol. 569, 1984.
[11] P. Gilliéron, F. Chometon, J. Laurent, Analysis of hysteresis and phase shifting phenomena in unsteady three-dimensional wakes, Exp. Fluids 35 (2003).
[12] H.E. Fieldler, H.H. Fernholz, On the management and control of turbulent shear flows, Prog. Aerosp. Sci. 27 (1990).
[13] P. Gilliéron, Contrôle des écoulements appliqué à l'automobile. Etat de l'art, Mec. Ind. 3 (6) (2002).
[14] E. Bideaux, P. Bobillier, E. Fournier, P. Gilliéron, M. El Hajem, J.Y. Champagne, P. Gilotte, A. Kourta, Aerodynamics for land vehicles; flow control; drag reduction with pulsed jets on thick body and massive flow separation, Int. J. Aerodyn. 1 (2011).
[15] P.W. Bearman, Investigation of the flow behind a two-dimensional model with a blunt trailing edge with splitter plates, J. Fluid Mech. 21 (1965).
[16] P.W. Bearman, J.K. Harvey, Control of circular flow by the use of dimples, AIAA J. 31 (1993).
[17] Y. Suzuki, T. Ijima, Profile drag of circular cylinders with surface roughness of straight knurls, Flucome 94 (1994).
[18] C.-H. Bruneau, I. Mortazavi, Passive control of the flow around a square cylinder using porous media, Internat. J. Numer. Methods Fluids 46 (2004) 415–433.
[19] C.-H. Bruneau, I. Mortazavi, P. Gilliéron, Passive control around the two-dimensional square back Ahmed body using porous devices, J. Fluids Eng. 130 (2008) 1–33.
[20] H. Lamb, Hydrodynamics, Cambridge University Press, 1916.

[21] L.M. Milne-Thomson, Theoretical Aerodynamics, Dover, 1966.
[22] L.M. Milne-Thomson, Theoretical Hydrodynamics, Dover, 1968.
[23] P. Angot, C.-H. Bruneau, P. Fabrie, A penalization method to take into account obstacles in incompressible viscous flows, Numer. Math. 81 (1999) 497–520.
[24] C.-H. Bruneau, P. Fabrie, Effective downstream boundary conditions for incompressible Navier–Stokes equations, Internat. J. Numer. Methods Fluids 19 (1994) 693–705.
[25] C.-H. Bruneau, M. Saad, The 2D lid-driven cavity problem revisited, Comput. Fluids 35 (2006) 326–348.
[26] D. Sipp, F. Coppens, L. Jacquin, Theoretical and numerical analysis of wake vortices, ESAIM Proc. 7 (1999).
[27] I. Mortazavi, A. Giovannini, The simulation of vortex dynamics downstream of a plate separator using a vortex-finite element method, Int. J. Fluid Dyn. 5 (2001).
[28] C. Basdevant, On the validity of the Weiss criterion in two-dimensional turbulence, Physica D 73 (1–2) (1994).
[29] M. Rouméas, P. Gilliéron, A. Kourta, Analysis and control of the near-wake flow over a square-back geometry, Comput. Fluids 38 (1) (2009).